

Coaxial vibrations of electrostatically actuated DWCNT resonators: Amplitude–voltage response of parametric resonance

Dumitru I. Caruntu^{*}, Ezequiel Juarez

University of Texas-Rio Grande Valley, Mechanical Engineering Department, Edinburg, TX 78539, USA

ARTICLE INFO

Keywords:

Double-wall carbon-nanotube resonators
Coaxial vibrations
Parametric resonance
Amplitude–voltage response
Reduced order model

ABSTRACT

This paper investigates the amplitude–voltage response of parametric resonance of coaxial vibrations of double-walled carbon nanotubes (DWCNTs) under electrostatic actuation. The system under investigation consists of a DWCNT parallel to a ground plate and under AC voltage. This voltage produces a nonlinear electrostatic force leading the DWCNT into vibrations. There is a nonlinear intertube van der Waals force between the two coaxial carbon-nanotubes. In coaxial vibration, the two concentric nanotubes move together synchronously. The AC frequency is near the fundamental coaxial natural frequency of the DWCNT. This leads to parametric resonance. The case of small damping, soft electrostatic actuation, and DWCNTs with a high length to diameter ratio (Euler–Bernoulli beam model), is considered. Modal analysis is performed to decouple the equations of free vibrations in their linear part. The solution of the nonlinear problem is then found in terms of modal coordinates. Reduced Order Models (ROMs) using from one to five modes of vibration are used for investigation. Three methods are used to solve these models, (1) the Method of Multiple Scales used to solve the ROM using one mode of vibration, (2) continuation and bifurcation analysis of the five modes of vibration (5T) Reduced Order Model (ROM) using AUTO-07P, and (3) numerical integration of 5T ROM using Matlab. All models and methods are in excellent agreement for amplitudes lower than 0.4 of the gap, while at amplitudes larger than 0.4 only 5T-ROM provide reliable results. The effects of detuning frequency and damping on the amplitude–voltage response of DWCNTs under electrostatic actuation are reported. The importance of the results in this paper are the effect of damping and detuning frequency on the subcritical and supercritical bifurcations, as they define the voltage intervals DWCNT reaches nonzero steady-state amplitudes.

1. Introduction

Within the field of Nano-Electro-Mechanical Systems (NEMS), Double-Walled Carbon Nanotubes (DWCNTs) constitute a growing research topic. DWCNTs have excellent mechanical and electrical properties, and they can be used as sensors [1–5], lasers [6–8], and nanoswitches and transistors [9,10]. For DWCNTs mass resonator sensors, one uses electrostatic actuation. Systems under this type of actuation experience a phenomenon of pull-in instability [3,11]. Free vibration response of coaxial vibrations of DWCNTs has been previously reported [3].

In many applications, DWCNTs' high electrical conductivity, thermal stability, and transmittance have made them a very good candidate over traditional materials. Hou et al. [10] reported the best performing DWCNTs as transparent conductive films. Manufactured via catalyst chemical vapor deposition method with sulfur as growth promoter and methane as carbon source, their DWCNTs displayed desirable electrical properties due to their long lengths and high structural integrity. Since the ability to mass produce high quality DWCNTs, NEMS researchers

have taken an interest in them as field-effect transistors (FETs). Liang and Wang [12] sought the opportunity to make use of the DWCNT's inner tube as a gate; they noted that due to the 0.34 nm spacing between the inner and outer tube, their design outperformed single-walled carbon nanotube FETs by providing better gate control.

Ouakad and Younis [13] estimated the natural frequencies and mode shapes of electrically actuated initially curved carbon nanotubes and investigated the role of various parameters affecting these frequencies. They used a 2D nonlinear curved CNT beam model to simulate the coupled in-plane and out-of-plane motions of the CNT. A ROM using a multimode Galerkin procedure was derived. They predicted “the transfer of energy among vibration modes involved in the veering phenomenon”.

Xu et al. [14] investigated the vibration of DWCNTs aroused by nonlinear intertube van der Waals forces. The inner and outer carbon nanotubes were modeled as elastic beams. The harmonic balance method was used to predict the relationship between the amplitudes of deflection and the frequencies of coaxial and noncoaxial free vibrations.

^{*} Corresponding author.

E-mail addresses: dumitru.caruntu@utrgv.edu, caruntud2@asme-member.org (D.I. Caruntu).

They reported that “van der Waals forces have a greater effect on the noncoaxial free vibrations than the coaxial free vibrations”.

Hajnayeb and Khadem [15] used Euler–Bernoulli beam theory to model clamped clamped DWCNTs under electrostatic actuation. Their model included linear damping, stretching terms, and nonlinear intertube van der Waals force, and electrostatic force due to AC and DC voltage. Using a perturbation method and long-time integration, they predicted amplitude–voltage responses under primary and secondary resonance conditions. DWCNTs experienced softening and hardening behavior depending on the value of DC voltage. When the AC frequency was at either coaxial or noncoaxial frequency, the other mode was “damped out in the steady-state response because of system damping”.

Caruntu and Juarez [3] reported the amplitude–frequency response of parametric resonance of coaxial transverse vibrations of electrostatically actuated DWCNT. They showed that “increasing voltage and/or decreasing damping resulted in a larger range of frequencies for which pull-in occurs”.

This work is an extension of Caruntu and Juarez [3]. To the best of our knowledge this is the first time when the amplitude–voltage response of parametric resonance of coaxial vibrations of electrostatically actuated DWCNT resonators is reported. The bifurcation diagram shows three bifurcations: subcritical, supercritical, and saddle–node. This indicates that there are cases in which the pull-in phenomenon cannot occur, which makes the DWCNT an excellent candidate for sensing applications. Sweeping up the voltage, the DWCNT from a zero steady-state amplitude suddenly jumps to a larger amplitude when reaching the subcritical bifurcation point. Sweeping down the voltage, the steady-state amplitude of the DWCNT increases to larger values after reaching the supercritical bifurcation point until reaching the saddle–node bifurcation point where then suddenly jumps to a zero amplitude. This behavior can be used as a sensing mechanism having the advantage that pull-in does not occur. The models and the methods of investigations are presented in more detail in Ref. [3], as well as the tables with data used for numerical simulations of present work. The DWCNT is electrostatically actuated with an AC frequency near the first coaxial natural frequency. The nonlinearities arise from the intertube van der Waals and electrostatic forces. Reduced order models (ROMs) [3,16–18] up to five modes (5T ROM) of vibration are used to transform the partial differential equation of motion into a system of ordinary differential equations. MMS of 1T ROM is also considered for analytical approximation [3,16]. Taylor polynomials are used to approximate the nonlinear electrostatic force. A modal coordinate transformation is used for both MMS and ROM, whereby a modal truncation provides a reduced model without loss of generality. Also, numerical integrations of ROMs (2T–5T ROM) of vibration are used to investigate the parametric resonance of coaxial vibrations of DWCNTs.

This is the first time when ROMs using up to five modes of vibration [3] have been used to investigate the amplitude–voltage response of parametric resonance of coaxial vibrations of electrostatically actuated DWCNT resonators. Lastly, the effects of detuning frequency and damping parameter on the DWCNT amplitude–voltage response are reported.

2. Differential equations of motion

The dimensionless partial differential equations describing the motion of the carbon nanotubes of the DWCNT are given by [3]:

$$\begin{cases} A^* \frac{\partial^2 w_1}{\partial \tau^2} + I^* \frac{\partial^4 w_1}{\partial z^4} = \bar{f}_{vdWT-T} \\ \frac{\partial^2 w_2}{\partial \tau^2} + \frac{\partial^4 w_2}{\partial z^4} = -b^* \frac{\partial w_2}{\partial \tau} - \bar{f}_{vdWT-T} + \delta \bar{f}_{elec} \cos^2 \Omega^* \tau \end{cases} \quad (1)$$

where z is the dimensionless longitudinal coordinate, τ dimensionless time, $w_1(z, \tau)$ and $w_2(z, \tau)$ are the dimensionless deflections of inner and outer CNTs, respectively, A^* dimensionless cross-section area, I^* dimensionless cross-section moment of inertia, b^* dimensionless damping, δ dimensionless voltage parameter, Ω^* dimensionless AC

frequency, \bar{f}_{vdWT-T} dimensionless intertube van der Waals force, and $\delta \bar{f}_{elec} \cos^2 \Omega^* \tau$ the electrostatic force acting on the outer CNT [14], where

$$\bar{f}_{vdWT-T} = C_1^*(w_2 - w_1) + C_3^*(w_2 - w_1)^3 \quad (2)$$

$$\bar{f}_{elec} = [(1 - w_2)^2 - s_2^2]^{-\frac{1}{2}} \ln^{-2} \left(\frac{1 - w_2}{s_2} + \sqrt{\frac{(1 - w_2)^2}{s_2^2} - 1} \right) \quad (3)$$

with $s_2 = R_2/g$ where g is the gap distance between the outer CNT and the ground plate, and C_1^* and C_3^* are the dimensionless coefficients linear and cubic terms of intertube van der Waals force. The dimensionless variables of Eqs. (1)–(3) are given by

$$w_n = \frac{y_n}{g}; \quad z = \frac{x}{\ell}; \quad \tau = \frac{t}{\ell^2} \sqrt{\frac{EI_2}{\rho A_2}} \quad (4)$$

where $n = 1, 2$, ℓ is the length of the DWCNT; x and t are the dimensional longitudinal coordinate and dimensional time, respectively; $y_1(x, t)$ and $y_2(x, t)$ are the dimensional deflections of inner and outer CNTs, respectively, E Young modulus, and ρ density. The dimensionless parameters of Eqs. (1)–(3) are as follows

$$\begin{aligned} A^* &= \frac{A_1}{A_2}, \quad I^* = \frac{I_1}{I_2}, \\ b^* &= \frac{b\ell^2}{\sqrt{\rho A_2 EI_2}}, \quad \delta = \frac{\pi \epsilon_0 \ell^4 V_0^2}{EI_2 g^2}, \quad \Omega^* = \Omega \ell^2 \sqrt{\frac{\rho A_2}{EI_2}}, \\ C_1^* &= \frac{C_1 \ell^4}{EI_2}, \quad C_3^* = \frac{C_3 g^2 \ell^4}{EI_2} \end{aligned} \quad (5)$$

where A_1 , I_1 and A_2 , I_2 are the cross-section areas and moments of inertia of the inner and outer CNTs, respectively, b damping per unit length, ϵ_0 permittivity of vacuum, Ω dimensional AC frequency, and C_1 and C_3 the linear and cubic intertube van der Waals coefficients, respectively [14], and V_0 the amplitude of the AC voltage. The values of the physical constants and dimensional parameters of the DWCNT can be found in Ref. [3].

A linear viscous damping model [3,19] under medium vacuum and room temperature conditions is considered. The viscous damping force is assumed to act only on the outer carbon nanotube. This assumption is based on the fact that the carbon nanotubes are modeled as concentric cylinders, and the intertube damping is negligible when compared to van der Waals intertube forces. The values for the physical constants and dry air conditions for viscous damping can be found in Ref. [3]. The electrostatic force acts only on the outer CNT (Faraday Cage Effect) [2,3,11,20,21].

3. Coaxial vibrations and AC frequency

Modal coordinates transformation: The intertube van der Waals force couples the two concentric CNTs. A Reduced Order Model (ROM) with one mode of vibration, $w_1 = u_1(\tau)\phi_1(z)$, $w_2 = v_1(\tau)\phi_1(z)$, where $\phi_1(z)$ is the first cantilever mode shape, and $u_1(\tau)$ and $v_1(\tau)$ are inner and outer tube functions of time, respectively, is used for the linearized system of partial differential equations of Eqs. (1). This linearized system describes DWCNT linear free vibrations. The linearized system of equations is then decoupled using modal coordinates r . The modal coordinate transformation for the DWCNT system is given by

$$\begin{bmatrix} u_1 & v_1 \end{bmatrix}^T = \begin{bmatrix} c & d \\ e & f \end{bmatrix} \begin{bmatrix} r_1 & r_2 \end{bmatrix}^T \quad (6)$$

where c , d , e , and f can be found in Ref. [3]. Afterwards, using these modal coordinates, the nonlinear Eqs. (1) become decoupled in their linear part as [3]

$$\ddot{r} + Ar = P^T M^{-\frac{1}{2}} F(r), \quad A = \begin{bmatrix} \bar{\omega}_1^2 & 0 \\ 0 & \bar{\omega}_2^2 \end{bmatrix} \quad (7)$$

where $r = [r_1 \ r_2]^T$, $\bar{\omega}_1 = 3.07309$ and $\bar{\omega}_2 = 29660.65309$ are the DWCNT’s coaxial and non-coaxial frequencies of resonance [3], and F

is the column matrix of applied forces of Eq. (1) after the substitution of modal coordinate transformation given by Eq. (6). To be able to use Eq. (7) with nonlinear terms, $w_1 = u_1(\tau)\phi_1(z)$ and $w_2 = v_1(\tau)\phi_1(z)$ are substituted into Eq. (1) which is then multiplied by the operator $\int_0^1 \cdot \phi_1(z) dz$. The following coefficients result $g_k = \int_0^1 \phi^{k+1}(z) dz$, [3,22]. The dimensional AC voltage in this work is as follows:

$$V = V_0 \cos \Omega t \tag{8}$$

where V_0 and Ω are the dimensional amplitude and dimensional circular frequency of the AC voltage, respectively.

In the case of parametric resonance of coaxial vibrations, the dimensionless AC frequency Ω^* is near first coaxial natural frequency $\bar{\omega}_1$

$$\Omega^* = \bar{\omega}_1 + \sigma \tag{9}$$

where σ is the detuning frequency. Since the electrostatic force is given by $\delta \bar{f}_{elec} \cos^2 \Omega^* \tau$ or $\delta \bar{f}_{elec} [1/2 + (e^{2i\Omega^* T_0} + e^{-2i\Omega^* T_0})/4]$, one can see that the frequency of the electrostatic force is twice the AC frequency, Eq. (9). Therefore, the resonance the DWCNT experiences is parametric resonance.

4. Methods of investigation

4.1. Method of multiple scales (MMS)

The dimensionless electrostatic force Eq. (3) is approximated using a Taylor polynomial as follows:

$$\bar{f}_{elec}(w_2) = \sum_{k=0}^3 \alpha_k w_2^k \tag{10}$$

Consider b^* and δ to be small, i.e. the system is under small damping and soft excitation. The intertube coefficients are large value parameters. Setting the small parameters to a slow time scale by multiplying them by a small dimensionless bookkeeping parameter ϵ , Eqs. (7) become:

$$\left\{ \begin{aligned} \ddot{r}_1 + \bar{\omega}_1^2 r_1 &= \epsilon C_3^* (er_1 + fr_2 - cr_1 - dr_2)^3 g_3 + \\ &e \left[C_3^* (cr_1 + dr_2 - er_1 - fr_2)^3 g_3 - \epsilon b^* (e\dot{r}_1 + f\dot{r}_2) \right. \\ &\left. + \epsilon \delta \sum_{k=0}^3 \alpha_k g_k (er_1 + fr_2)^k \cos^2 \Omega^* \tau \right] \\ \ddot{r}_2 + \bar{\omega}_2^2 r_2 &= \epsilon C_3^* (er_1 + fr_2 - cr_1 - dr_2)^3 g_3 + \\ &f \left[C_3^* (cr_1 + dr_2 - er_1 - fr_2)^3 g_3 - \epsilon b^* (e\dot{r}_1 + f\dot{r}_2) \right. \\ &\left. + \epsilon \delta \sum_{k=0}^3 \alpha_k g_k (er_1 + fr_2)^k \cos^2 \Omega^* \tau \right] \end{aligned} \right. \tag{11}$$

where the values of coefficients α_k can be found in Ref. [3]. Consider fast $T_0 = \tau$ and slow $T_1 = \epsilon \tau$ time scales, and first-order expansions of r_1 and r_2 as follows:

$$\begin{cases} r_1 = r_{10} + \epsilon r_{11} \\ r_2 = r_{20} + \epsilon r_{21} \end{cases} \tag{12}$$

where r_{10} , r_{20} , and r_{11} , r_{21} are the zero-order and first-order approximation solutions, respectively [3,14]. A first-order expansion for each displacement in Eq. (12) gives good results. There is no need to go for higher-order expansions. The time derivative is then expressed in terms of derivatives with respect to the fast and slow scales. Substituting Eqs. (12) into Eq. (11) two problems result, namely, zero-order problem

and first-order problem [3]. For the zero-order problem consider r_{10} and r_{20} to be as follows:

$$\begin{cases} r_{10} = p(T_1) [e^{i\omega T_0} + e^{-i\omega T_0}] \\ r_{20} = q(T_1) [e^{i\omega T_0} + e^{-i\omega T_0}] \end{cases} \tag{13}$$

and use the Harmonic Balance Method (HBM) [3,14]. Solving for amplitudes p and q yields to the amplitude–frequency response of the zero-order MMS problem. DWCNT free vibrations of coaxial vibrations and noncoaxial vibrations have been previously investigated [3,14]. In the case of coaxial vibrations $u_1 = u_2$. This leads to:

$$e \cdot r_{10} + f \cdot r_{20} - c \cdot r_{10} - d \cdot r_{20} = 0 \tag{14}$$

In the case of parametric resonance of coaxial vibrations, the dimensionless AC frequency Ω^* is near coaxial frequency $\bar{\omega}_1$, Eq. (9). For MMS this results into

$$\Omega^* T_0 = \bar{\omega}_1 T_0 + \sigma T_1 \tag{15}$$

where σ is the detuning frequency. Substituting Eqs. (13)–(15) into the first-order problem, collecting the secular terms, and set the derivatives with respect to the slow time scale equal to zero leads to the steady-state solutions [3]. The amplitude–voltage steady-state solutions a_1 , δ are zero amplitude solutions for the entire range of voltage investigated, and nonzero amplitude solutions given by

$$a_1 = \sqrt{\frac{8e^2 b^* \bar{\omega}_1}{\alpha_3 \delta e^4 g_3} \cdot \frac{1}{\sin 2\gamma} - \frac{2\alpha_1 g_1}{\alpha_3 e^2 g_3}} \tag{16}$$

$$\sigma = -\frac{\alpha_1 \delta e^2 g_1}{8\bar{\omega}_1} (2 + \cos 2\gamma) - \frac{\alpha_3 \delta e^4 g_3}{16\bar{\omega}_1} [3 + 2 \cos 2\gamma] a_1^2 \tag{17}$$

where

$$\gamma = \sigma T_1 - \beta \tag{18}$$

and

$$p = \frac{1}{2} a_1 e^{i\beta}, \quad q = \frac{1}{2} a_2 e^{i\beta} \tag{19}$$

4.2. Reduced order model (ROM)

Reduced Order Models (ROMs) with two or more modes of vibration are used in this paper. Eq. (1) can be written as

$$\begin{cases} A^* \frac{\partial^2 w_1}{\partial \tau^2} + I^* \frac{\partial^4 w_1}{\partial z^4} = \bar{f}_{vdWT-T} \\ \frac{\partial^2 w_2}{\partial \tau^2} + \frac{\partial^4 w_2}{\partial z^4} = -b^* \frac{\partial w_2}{\partial \tau} - \bar{f}_{vdWT-T} + \frac{\delta \cos^2 \Omega^* \tau}{\sum_{k=0}^5 a_k w_2^k} \end{cases} \tag{20}$$

where f_{elec} was replaced by a fifth-degree Taylor polynomial at the denominator [3,23]. ROMs with larger number of modes of vibration have been reported to be accurate for strong nonlinearities and high amplitudes [18]. The solutions of the dimensionless deflections are assumed as follows

$$\begin{cases} w_1(z, \tau) = \sum_{i=1}^N [c_i \cdot r_{1i}(\tau) + d_i \cdot r_{2i}(\tau)] \phi_i(z) \\ w_2(z, \tau) = \sum_{i=1}^N [e_i \cdot r_{1i}(\tau) + f_i \cdot r_{2i}(\tau)] \phi_i(z) \end{cases} \tag{21}$$

where N is the number of ROM terms (modes of vibration), ϕ_i are cantilever mode shapes, and $r_{1i}(\tau)$ and $r_{2i}(\tau)$ are the time functions to be determined. Note that $z = 1$ characterizes the tip of the cantilevered structure. Modal truncation has been reported in the literature, i.e. the amplitudes of the non-resonant mode (noncoaxial in this case) are negligible [3,15]. In present work only $r_{1i}(\tau)$, $i = 1, 2, \dots, N$, modal coordinates are significant. Therefore, for numerical efficiency, without loss of generality, Eq. (20) after a modal coordinate transformation,

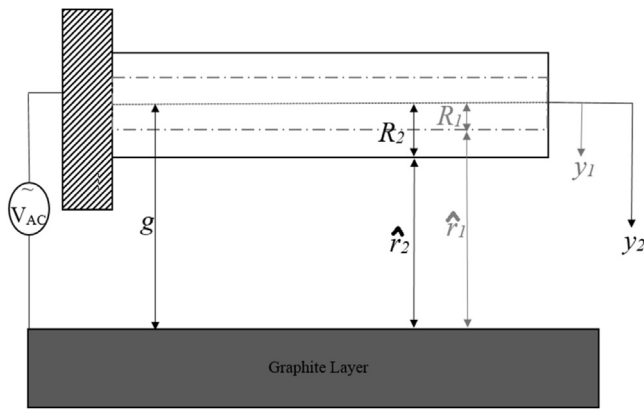


Fig. 1. Electrostatically actuated DWCNT cantilever to include damping and intertube van der Waals forces [3].

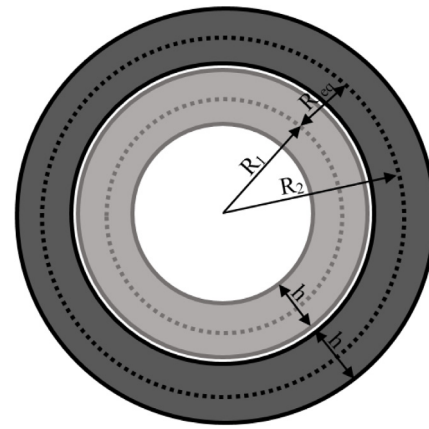


Fig. 2. DWCNT Cross Section [3].

modal truncation of $r_{2i}(\tau)$, and multiplication of the denominator at the right-hand side [3], becomes

$$\begin{aligned} & \sum_{i=1}^N \frac{\partial^2 r_{1i}}{\partial \tau^2} \left(\sum_{j_1=1}^N a_0 h_{nj_1} + \sum_{k=1}^5 a_k \sum_{j_2 \dots j_k=1}^N e_{j_2 \dots j_k} r_{1j_2 \dots j_k} h_{nj_1 j_2 \dots j_k} \right) = \\ & -b^* \sum_{i=1}^N e_i^2 \frac{\partial r_{1i}}{\partial \tau} \left(\sum_{j_1=1}^N a_0 h_{nj_1} + \sum_{k=1}^5 a_k \sum_{j_2 \dots j_k=1}^N e_{j_2 \dots j_k} r_{1j_2 \dots j_k} h_{nj_1 j_2 \dots j_k} \right) \\ & - \sum_{i=1}^N \bar{\omega}_{1i}^2 r_{1i} \left(\sum_{j_1=1}^N a_0 h_{nj_1} + \sum_{k=1}^5 a_k \sum_{j_2 \dots j_k=1}^N e_{j_2 \dots j_k} r_{1j_2 \dots j_k} h_{nj_1 j_2 \dots j_k} \right) \\ & + \sum_{i=1}^N e_i \delta h_n \cos^2 \Omega^* \tau \end{aligned} \quad (22)$$

where $n = 1, 2, \dots, N$, and $j_1, j_2, \dots, j_k = 1, 2, \dots, N$. The values of a_k coefficients can be found in Ref. [3]. Coefficients h are as follows:

$$\begin{aligned} h_n &= \int_0^1 \phi_n dz, h_{nj_1} = \int_0^1 \phi_{j_1} \phi_n dz, h_{nj_1 j_2} = \int_0^1 \phi_{j_1} \phi_{j_2} \phi_n dz \dots h_{nj_1 j_2 \dots j_k} \\ &= \int_0^1 \phi_{j_1} \phi_{j_2} \dots \phi_{j_k} \phi_n dz \end{aligned} \quad (23)$$

It should be noted that $h_{ni} = \delta_{ni}$, where δ_{ni} is Kronecker's delta.

5. Numerical simulations

The data used for numerical simulations of present work dealing with parametric resonance of coaxial vibrations of electrostatically actuated DWCNT, Figs. 1 and 2, can be found in Ref. [3]. ROM with five modes of vibration has been solved using AUTO-07P, a software package for continuation and bifurcation, in order to predict the amplitude-voltage response. The same ROM was numerically integrated using the MATLAB solver ode15s, a ‘‘multistep, variable order solver based on numerical differentiation formulas’’ [24,25], in order to predict time responses of the system. Also MMS was used in this investigation. MMS is a perturbation technique [26,27] that is utilized due to the ease of identifying amplitude-voltage responses for weak nonlinearities and low amplitudes. MMS provides an approximate analytical solution for ROM with one mode of vibration. To investigate solutions of higher amplitude and verify those of smaller amplitude, ROMs with a larger number of modes of vibration have been used. While more accurate at higher amplitudes, ROMs are more time-consuming.

Fig. 3 shows the amplitude-voltage response of the parametric resonance of coaxial vibrations of DWCNT using 5T ROM AUTO, MMS, and 5T ROM time responses from initial amplitudes of $U_0 = 0$ and $V_0 = 0.5$. In the horizontal axis is the dimensionless voltage parameter δ , and in the vertical axis the dimensionless steady-state amplitudes U_{max} and V_{max} of the free ends of the inner and outer carbon nanotubes, respectively. U_{max} and V_{max} are equal in the case of coaxial vibrations.

Dash and solid lines represent the unstable and stable solutions, respectively. This response is characterized by two bifurcations at zero amplitude, subcritical bifurcation point A and supercritical bifurcation point B, and another bifurcation point C in higher amplitudes. For any initial amplitude and any given dimensionless voltage δ to the left of bifurcation point C and to the right of supercritical bifurcation point B, the amplitude will settle to zero. Conversely, for any initial amplitude less than 1 and any voltage between the bifurcation points A and B, the amplitude will settle on the higher amplitude stable branch BC. For voltage between the bifurcation points A and C, depending on the initial amplitude U_0 , the amplitude of DWCNT will settle to zero or an amplitude on the stable branch BC.

In the case of the voltage being swept up, the DWCNT experiences a zero steady-state amplitude until the subcritical bifurcation point A is reached. Here, the DWCNT loses stability and it experiences a sudden jump up in amplitude to about 0.8 of the gap on branch BC. Next, the steady-state amplitude decreases along branch BC until it reaches a zero value at the supercritical bifurcation point B, and then remains at this value. In the case of the voltage being swept down, the steady-state amplitude is zero, and it remains zero until it reaches bifurcation point B. Then the amplitude increases along branch BC until it reaches the bifurcation point C. At this point, the DWCNT loses stability and the amplitude suddenly jumps down to zero, and stays zero as the voltage continues to be swept down.

The ROM and MMS predictions are in excellent agreement for amplitudes less than 0.4 of the gap. For amplitudes larger than 0.4 of the gap, MMS fails to accurately predict the behavior of the system. MMS fails to predict the bifurcation point C that occurs at higher amplitudes, and it underestimates the softening effect. This is expected since MMS is a method valid for weak nonlinearities and small to moderate amplitudes.

Fig. 4 illustrates the convergence of the ROMs with respect to the number of the modes of vibration of the ROM. Numerical simulations using AUTO-07P, shows the amplitude-voltage responses for numbers of modes of vibrations in the ROM between two and five. One can see that there is no significant difference between 4T ROM AUTO and 5T ROM AUTO for all amplitudes. The 2T ROM AUTO solutions show a significant difference in predicting the bifurcation points, indicative of low accuracy when not enough terms are considered. There is no need to check for higher terms above 5T ROM since five terms is shown to be appropriate for accurate predictions.

Fig. 5 shows that the solution converges with the increase of the degree of the Taylor polynomial in the denominator for 5T ROM, Eq. (20). Similar to the term convergence shown in Fig. 4, a numerical solution convergence may be seen in the fifth degree of the Taylor polynomial of the electrostatic force in the denominator, with an excellent approximation of higher steady-states amplitudes.

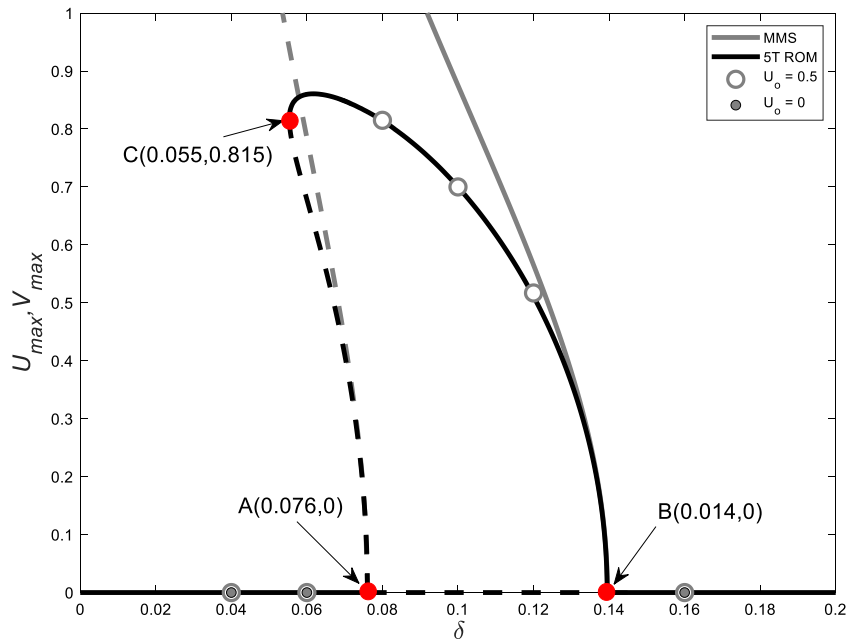


Fig. 3. Parametric resonance of DWCNT coaxial vibrations; amplitude-voltage response using MMS, five terms (5T) ROM AUTO with a 5th degree Taylor polynomial in the denominator, Eq. (20), and five terms (5T) ROM Time Responses with a 5th degree Taylor polynomial, $b^* = 0.00035$, $\sigma = -0.00025$.

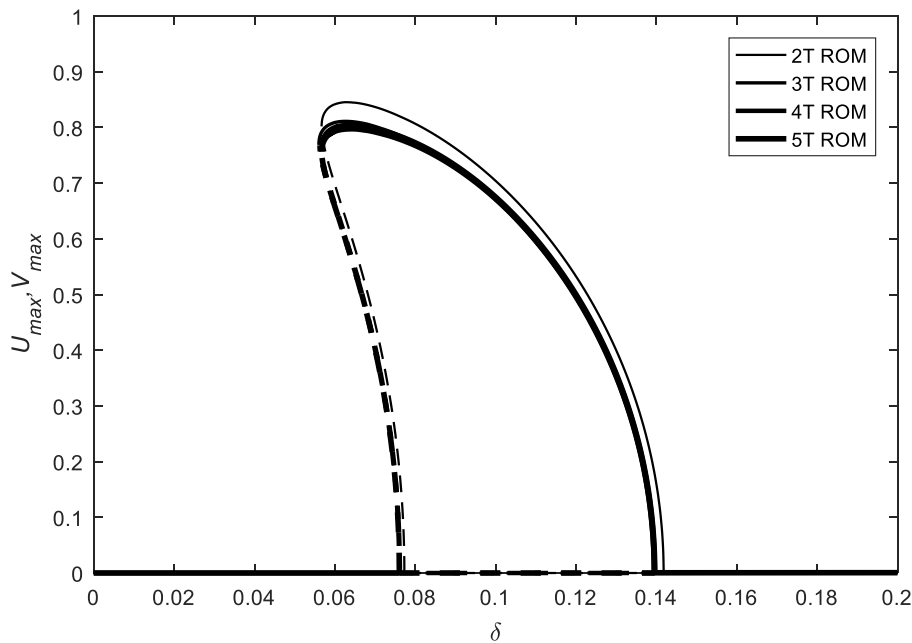


Fig. 4. Convergence of the amplitude-voltage response for DWCNT resonator using two terms (2T ROM AUTO), three terms (3T ROM AUTO), ..., and five terms (5T ROM AUTO), and a second degree Taylor polynomial in the denominator, Eq. (20), $b^* = 0.00035$, $\sigma = -0.00025$.

Fig. 6(a–d) show time responses using 5T ROM for $b^* = 0.00035$ and $\sigma = -0.00025$ considering various initial amplitudes and values of voltage, where $u = w_1(1, \tau)$ and $v = w_2(1, \tau)$. They are in excellent agreement with the voltage response from 5T ROM AUTO, as shown in Fig. 3. Fig. 6(a–b) characterize the behavior to the left of the subcritical bifurcation point A, where regardless of initial amplitude, the DWCNT will settle to zero amplitude stable solution. Similarly, Fig. 6(d) shows the behavior to the right of the supercritical bifurcation point B, where regardless of initial amplitude, the deflections will reach zero amplitude. Fig. 6(c) shows the typical behavior of deflections in between the two subcritical and supercritical bifurcation points A and B, respectively, where the amplitudes will settle at the higher amplitude stable branch BC.

Fig. 7 shows the effect of detuning frequency σ on the amplitude-voltage response. Increasing the detuning frequency causes the supercritical bifurcation point B to significantly shift to lower voltages. The bifurcation point C is shifted to lower amplitudes and higher voltage. Furthermore, the voltage interval between the subcritical and supercritical bifurcation points A and B, leading to nonzero steady-state amplitudes decreases with the increase of detuning frequency.

Fig. 8 illustrates the effect of damping b^* on the amplitude-voltage response. Increasing damping on the electrostatically actuated DWCNT shifts the subcritical bifurcation point A to larger voltages and the supercritical bifurcation point B to lower voltages. Essentially, increasing damping reduces the voltage interval leading to nonzero steady-state amplitudes. It also reduces the value of the peak amplitude.

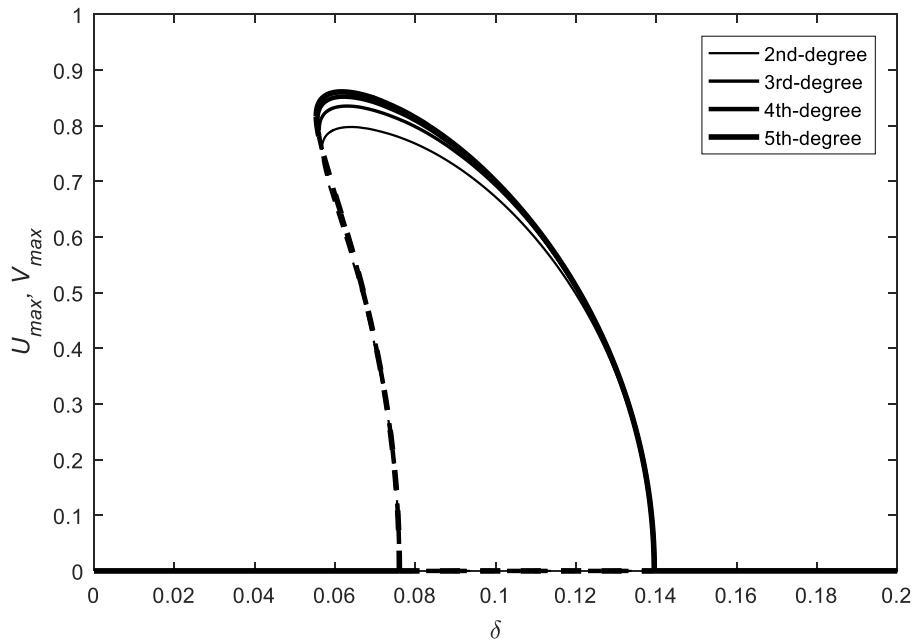


Fig. 5. Convergence of the amplitude–voltage response (5T ROM AUTO) of the DWCNT resonator using denominator Taylor polynomial from second to fifth degrees, $b^* = 0.00035$, $\sigma = -0.00025$.

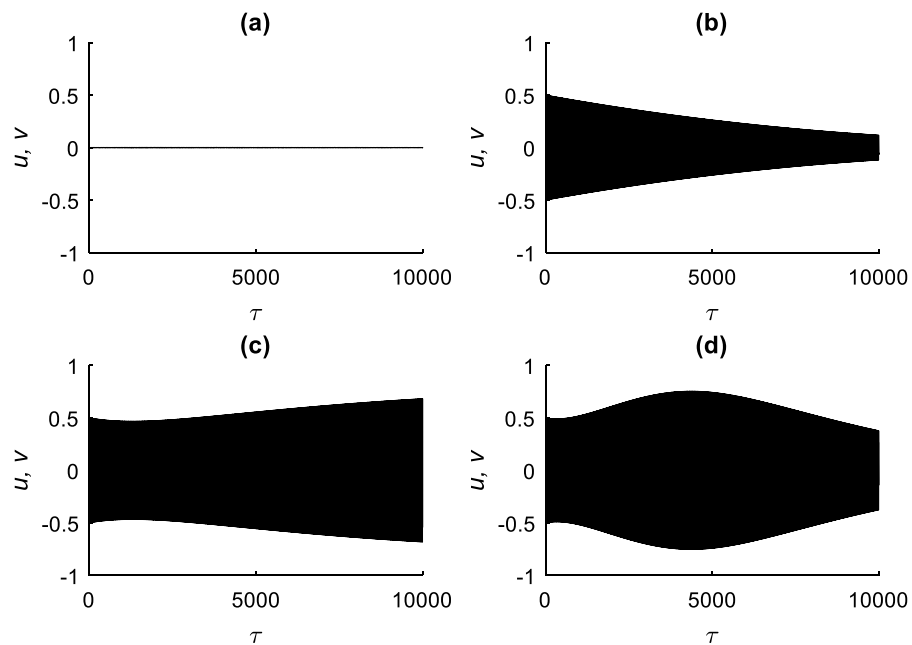


Fig. 6. 5T ROM time responses, $b^* = 0.00035$, $\sigma = -0.00025$, (a) Initial amplitude $U_0 = 0$, $\delta = 0.04$, (b) Initial amplitude $U_0 = 0.5$, $\delta = 0.04$, (c) Initial amplitude $U_0 = 0.5$, $\delta = 0.1$, (d) Initial amplitude $U_0 = 0.5$, $\delta = 0.16$.

6. Discussion and conclusions

This work deals with amplitude–voltage of coaxial parametric resonance of electrostatically actuated cantilever DWCNTs to include the intertube van der Waals forces. The amplitude–voltage response and the effects of detuning frequency and damping on the response were predicted. ROMs using from one to five modes of vibration were developed in order to investigate the response. ROM with one mode of vibration was solved using MMS. ROMs with two to five modes of vibration were solved using AUTO-07P, a software for continuation and bifurcation. Both methods predicted the response. Also, the ROM with five modes of vibration was numerically integrated using MATLAB

for predicting time responses of the system [16–18,22,28]. All three methods were in agreement for amplitudes lower than 0.4 of the gap. For amplitudes larger than 0.4 of the gap, only ROM using five modes of vibration predicted accurately the amplitude–voltage response of the DWCNT. The effects of damping and detuning frequency on the subcritical and supercritical bifurcation points *A* and *B* are important as these points define the interval of voltage for which DWCNT reaches nonzero steady-state amplitudes.

Notice that while MMS, and ROMs solved using AUTO provide only steady-state solutions, the ROMs solved using Matlab, i.e. numerical integration, provide time responses which include a transient response that settles to a steady-state amplitude.

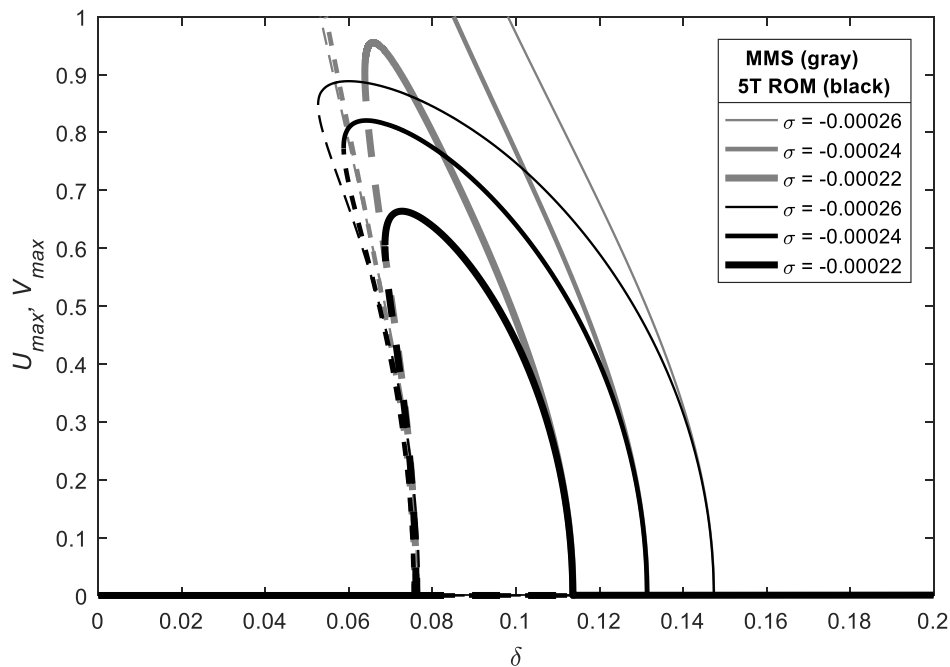


Fig. 7. Effect of detuning frequency σ on voltage response, MMS and 5T ROM AUTO, fifth degree Taylor polynomial in the denominator, Eq. (20), $b^* = 0.00035$.

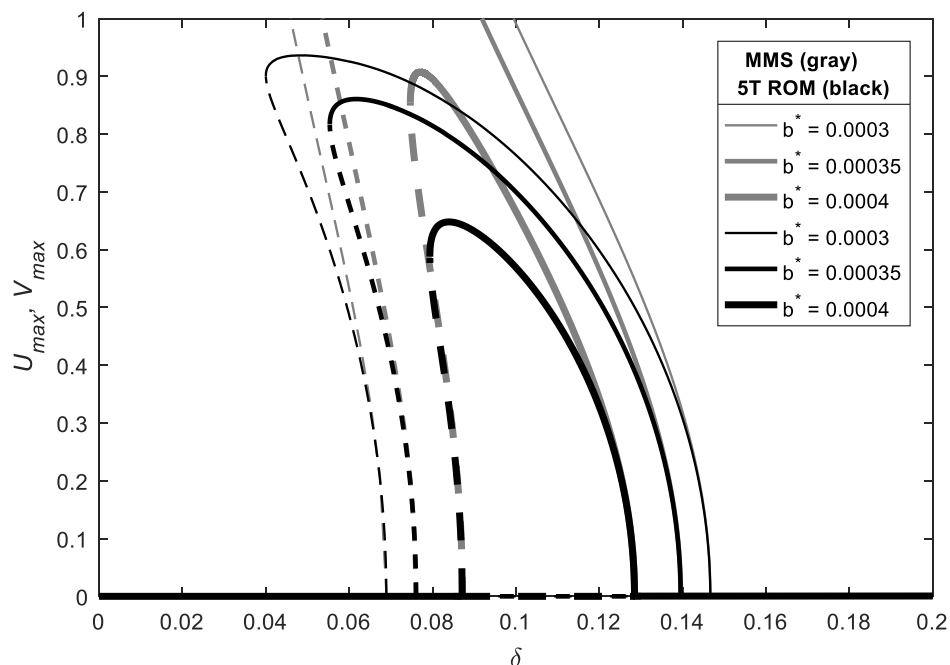


Fig. 8. Effect of dimensionless damping b^* on voltage response, MMS and 5T ROM AUTO, fifth degree Taylor polynomial in the denominator, Eq. (20), $\sigma = -0.00025$.

The amplitude–voltage response of parametric resonance of electrostatically actuated microelectromechanical system (MEMS) cantilever resonators (not DWCNTs) was recently investigated by Caruntu et al. [29]. ROM convergence and influences of detuning frequency and damping were similarly investigated. While the amplitude–voltage responses display similar nonlinear and stability behavior for parametric resonance of MEMS cantilevers and coaxial transverse vibrations of DWCNTs, for the same dimensionless amplitudes (with respect to the gap distance), the following differences are noted: (1) the values of detuning frequencies, to produce similar amplitudes in the amplitude–voltage response, are about 50 times smaller for DWCNT than MEMS cantilevers, (2) similarly the values of damping are about 100 times smaller, and (3) there

is a smaller range of voltages between the subcritical and supercritical bifurcation points A and B that will result in steady-state non-zero amplitudes. While MMS and ROM are similarly used, the novelty of this work lies in the application of modal coordinate transformation, modal truncation, and a different electrostatic force model for MWCNTs that involves a Taylor expansion in the denominator in ROM.

Similar modeling for an electrostatically actuated SWCNT has been previously investigated, where molecular dynamics (MD) and nonlocal beam modeling are compared to Euler–Bernoulli continuum beam theory [23]. This modeling has been shown to be valid for long slender CNTs. A model limitation is that this work does not investigate thermal vibrations [30].

Recent developments on Casimir force (another quantum dynamics effect besides van der Waals force) influence on NEMS cantilever resonators response (frequency–amplitude) have been reported in the literature [31].

Declaration of competing interest

The authors declare that they have no known competing financial interests or personal relationships that could have appeared to influence the work reported in this paper.

References

- [1] A.M. Patel, A.Y. Joshi, Vibration analysis of double wall carbon nanotube based resonators for septogram level mass recognition, *Comput. Mater. Sci.* 79 (2013) 230–238.
- [2] M.C. Ncibi, M. Sillanpaa, Optimized removal of antibiotic drugs from aqueous solutions using single, double and multi-walled carbon nanotubes, *J. Hazard. Mater.* 298 (2015) 102–110.
- [3] D.I. Caruntu, E. Juarez, Voltage effect on amplitude–frequency response of parametric resonance of electrostatically actuated double-walled carbon nanotube resonators, *Nonlinear Dynam.* 98 (4) (2019) 3095–3112, <http://dx.doi.org/10.1007/s11071-019-05057-8>.
- [4] K. Kiani, Vibration analysis of elastically restrained double-walled carbon nanotubes on elastic foundation subjected to axial load using nonlocal shear deformable beam theories, *Int. J. Mech. Sci.* 68 (2013) 16–34.
- [5] E. Meunier, et al., Double-walled carbon nanotubes trigger IL-1 β release in human monocytes through Nlrp3 inflammasome activation, *Nanomed. Nanotechnol. Biol. Med.* 8 (2012) 987–995.
- [6] E.V. Santiago, S.H. Lopez, M.A. Camacho Lopez, D.R. Contreras, R. Farias-Mancilla, S.G. Flores-Gallardo, C.A. Hernandez-Escobar, E.A. Zaragoza-Contreras, Optical properties of carbon nanostructures produced by laser irradiation on chemically modified multi-walled carbon nanotubes, *Opt. Laser Technol.* 84 (2016) 53–58.
- [7] S.M. Azooz, M.H.M. Ahmed, F. Ahmad, B.A. Hamida, S. Khan, H. Ahmad, S.W. Harun, Passively Q-switched fiber lasers using a multi-walled carbon nanotube polymer composite based saturable absorber, *Opt. - Int. J. Light Electron. Opt.* 126 (21) (2015) 2950–2954.
- [8] H. Yu, L. Zhang, Y. Wang, S. Yan, W. Sun, J. Li, Y. Tsang, X. Lin, Sub-100 ns solid-state laser Q-switched with double wall carbon nanotubes, *Opt. Commun.* 306 (2013) 128–130.
- [9] V.V. Deshpande, H.-Y. Chiu, H.W.C. Postma, C. Mikó, L. Forró, M. Bockrath, Carbon nanotube linear bearing nanoswitches, *Nano Lett.* 6 (6) (2006) 1092–1095.
- [10] A. Bartolomeo, M. Rinzan, A.K. Boyd, Y. Yang, L. Guadagno, F. Giubileo, P. Barbara, Electrical properties and memory effects of field-effect transistors from networks of single- and double-walled carbon nanotubes, *Nanotechnology* 21 (11) (2010) 115204.
- [11] M. Dequesnes, S.V. Rotkin, N.R. Aluru, Calculation of pull-in voltages for carbon nanotube based nanoelectromechanical switches, *Nanotechnology* 13 (2002) 120–131.
- [12] Y.X. Liang, T.H. Wang, A double-walled carbon nanotube field-effect transistor using the inner shell as its gate, *Phys. E Low-Dimens. Syst. Nanostruct.* 23 (1–2) (2004) 232–236.
- [13] H. Ouakad, M.I. Younis, Natural frequencies and mode shapes of initially curved carbon nanotube resonators under electric excitation, *J. Sound Vib.* 330 (2011) 3182–3195.
- [14] K.Y. Xu, X.N. Guo, C.Q. Ru, Vibration of double-walled carbon nanotube aroused by nonlinear intertube van der Waals forces, *J. Appl. Phys.* 99 (2006) 064303.
- [15] A. Hajnayeb, S.E. Khadem, Nonlinear vibration and stability analysis of double-walled carbon nanotube under electrostatic actuation, *J. Sound Vib.* 331 (2012) 2443–2456.
- [16] D.I. Caruntu, M. Botello, C.A. Reyes, J. Beatriz, Voltage response of superharmonic resonance of second order of electrostatically actuated MEMS cantilever resonators, *J. Comput. Nonlinear Dyn.* 14 (2019) 031005, <http://dx.doi.org/10.1115/1.4042017>, 8.
- [17] D.I. Caruntu, R. Oyervides, Frequency response reduced order model of primary resonance of electrostatically actuated MEMS circular plate resonators, *Commun. Nonlinear Sci. Numer. Simul.* 43 (2017) 261–270.
- [18] D.I. Caruntu, L. Luo, Bifurcation and pull-in voltages of primary resonance of electrostatically actuated CNT cantilevers to include van der Waals effect, *MECCANICA* 52 (2016) 849–859, <http://dx.doi.org/10.1007/s11012-016-0461-8>.
- [19] R.B. Bhiladvala, Z.J. Wang, Effects of fluids on the q factor and the resonance frequency of oscillating micrometer and nanometer scale beams, *Phys. Rev. E* 69 (2004) 036307.
- [20] Jackson J.D., *Classical Electrodynamics*, third ed., Wiley, New York, 1998.
- [21] G. Chen, S. Bandow, C. Margine, A.N. Kolmogorov, V.H. Crespi, R. Gupta, G.U. Sumanasekera, S. Ijima, P.C. Eklund, Chemically doped double-walled carbon nanotubes: Cylindrical molecular capacitors, *Phys. Rev. Lett.* 90 (25) (2013).
- [22] D.I. Caruntu, M. Knecht, MEMS cantilever resonators under soft AC voltage of frequency near natural frequency, *J. Dyn. Syst. Meas. Control* 137 (2015) 041016-1.
- [23] D.I. Caruntu, L. Luo, Frequency response of primary resonance of electrostatically actuated CNT cantilevers, *Nonlinear Dynam.* 78 (2014) 1827–1837.
- [24] L.F. Shampine, M.W. Reichelt, The MATLAB ODE suite, *SIAM J. Sci. Comput.* 18 (1997) 1–22.
- [25] L.F. Shampine, M.W. Reichelt, J.A. Kierzenka, Solving index-1 DAEs in MATLAB and simulink, *SIAM Rev.* 41 (3) (1999) 538–552.
- [26] Ali H. Nayfeh, Dean T. Mook, *Nonlinear Oscillations*, John Wiley & Sons, 2008.
- [27] A.H. Nayfeh, M.I. Younis, E.M. Abdel-Rahman, Dynamic pull-in phenomenon in MEMS resonators, *Nonlinear Dynam.* 48 (2007) 153–163.
- [28] D.I. Caruntu, R. Oyervides, Voltage response of primary resonance of electrostatically actuated MEMS clamped circular plate resonators, *J. Comput. Nonlinear Dyn.* 11 (2016) 041021, 7.
- [29] D.I. Caruntu, I. Martinez, M.W. Knecht, Parametric resonance voltage response of electrostatically actuated micro-electro-mechanical system cantilever resonators, *J. Sound Vib.* 362 (2016) 203–213.
- [30] L.F. Wang, H.Y. Hu, Thermal vibration of a simply supported single-walled carbon nanotube with thermal stress, *Acta Mech.* 227 (7) 1957–1967.
- [31] D.I. Caruntu, C.A. Reyes, Casimir effect on amplitude–frequency response of parametric resonance of electrostatically actuated NEMS cantilever resonators, in: B.E. Abali, I. Giorgio (Eds.), Chapter 15 in *Developments and Novel Approaches in Nonlinear Solid Body Mechanics – Book Series Advanced Structured Materials*, vol. 132, Springer Nature Switzerland AG, Gewerbestrasse 11, 6330, Cham, Switzerland, 2020, pp. 237–259, http://dx.doi.org/10.1007/978-3-030-50464-9_15, 2021.